Journal of Hazardous Materials 181 (2010) 986–995

Contents lists available at ScienceDirect

Journal of Hazardous Materials

journal homepage: www.elsevier.com/locate/jhazmat

# A novel cellulose–manganese oxide hybrid material by *in situ* soft chemical synthesis and its application for the removal of Pb(II) from water

Shihabudheen M. Maliyekkal, Kinattukara P. Lisha, T. Pradeep*

*DST Unit on Nanoscience, Department of Chemistry and Sophisticated Analytical Instrument Facility, Indian Institute of Technology Madras, Chennai 600036, India*

ARTICLE INFO

*Article history:*
Received 16 March 2010
Received in revised form 17 May 2010
Accepted 21 May 2010
Available online 31 May 2010

*Keywords:*
Adsorption
Cellulose
Hybrid materials
Lead
Nanoscale-manganese oxide

ABSTRACT

We report an *in situ* soft chemical synthesis of a novel hybrid material, cellulose–nanoscale-manganese oxide composite (C–NMOC), and its application for Pb(II) removal from aqueous solutions. For comparison, detailed Pb(II) adsorption studies were also performed with nanoscale-manganese oxide powder (NMO), prepared through a similar route. Various spectroscopic and microscopic techniques were used to characterize the as-synthesized materials. X-ray photoelectron spectroscopic (XPS) measurements confirmed the existence of Mn(IV) phase in NMO whereas C–NMOC showed largely the Mn(III) phase. The existence and uniform distribution of manganese oxide in cellulose fiber materials was confirmed by SEM and EDAX analyses. The adsorption studies reveal that the Pb(II) uptake onto C–NMOC is a fast process and >90% of the uptake occurred within the first 10 min contact time. The Sips isotherm predicted the equilibrium data well and the maximum Pb(II) uptake capacity of C–NMOC (4.64% Mn loading) was estimeted to be 80.1 mg $g^{-1}$. The Pb(II) adsorption capacity of C–NMOC (per gram of Mn present) was several times higher than commercial manganese oxide (β-$MnO_2$) and at least twice larger than NMO. The experimental evidence reveals that physisorption plays a dominant role in Pb(II) adsorption by both NMO and C–NMOC.



## 1. Introduction

Presence of heavy metals in water continues to be a major concern because of their toxicity, accumulation in the food chain and persistence in nature. Lead is one such heavy metal, which induces a multitude of physiological, biochemical, and behavioral dysfunctions; particularly in children [1]. Among the top 20 hazardous substances elaborated by the Agency for Toxic Substances and Disease Registry (ATSDR) and the U.S. Environmental Protection Agency (USEPA), lead occupies the second place, just below arsenic [2]. Manufacture of storage batteries, paints and pigments, oil, fertilizers, ammunition, solder, plumbing fixtures, ceramics, glass, cable coverings, radioactivity shields, lead smelting and mining are the important industrial activities that contribute lead into the aqueous medium [3–5]. Concentration of lead ions in many industrial waters was reported to be as high as 200–500 mg $l^{-1}$, which is very high in relation to the current water quality standard of 0.1–0.05 mg $l^{-1}$ [6]. Hence, it is mandatory to reduce the lead levels in drinking water, wastewater and water used for agriculture to the maximum permissible concentration.

Though various physicochemical and biological methods have been developed for removing lead from contaminated waters, it is best accomplished by adsorption on suitable adsorbents [5,7]. At present, numerous sorbents have been tested for metal removal from aqueous medium. Manganese oxides have been a subject of interest in various fields including molecular adsorption due to their outstanding structural multiformity combined with novel chemical and physical properties [8]. Besides the ability to remove a wide range of ions from wastewater, manganese oxides are interesting in environmental remediation because of their low cost, less toxicity and wide availability.

With the emergence of nanoscience and technology in the last decade, research has been initiated to exploit the unusual and unique properties of nanomaterials for environmental remediation [9–11]. Various methods of synthesis of manganese oxides are available in the literature and the products are known to show different physical and chemical properties. Among the various methods available for controlled synthesis, the "soft chemistry" routes, which are based on solution phase processes, are effective for the synthesis of nanostructured materials with well-controlled shapes, sizes, and structures [12,13]. Recent investigation shows that various nanostructured manganese oxides can be prepared through a simple route by the reduction of $KMnO_4$ by organic acids or alcohols [14,15]. The methodologies adopted in these syntheses are interesting because they are simple, fast, low cost and eco-friendly. The process involves only one manganese precursor, $KMnO_4$, simplifying the post-synthesis treatment and thereby increasing the viability in commercial applications. However, the

* Corresponding author. Tel.: +91 44 2257 4208; fax: +91 44 2257 0545.
*E-mail address:* pradeep@iitm.ac.in (T. Pradeep).

0304-3894/$ – see front matter © 2010 Elsevier B.V. All rights reserved.
doi:10.1016/j.jhazmat.2010.05.112

**Nomenclature**

| | |
|---|---|
| $b_L$ | Langmuir isotherm constant ($l\,mg^{-1}$) |
| $C_e$ | equilibrium concentration of Pb(II) in the solution ($mg\,l^{-1}$) |
| $E_{DR}$ | mean free energy of adsorption ($kJ\,mol^{-1}$) |
| $k_1$ | first-order rate constant of adsorption ($min^{-1}$) |
| $k_2$ | second-order rate constant of adsorption ($g\,mg^{-1}\,min^{-1}$) |
| $K_d$ | distribution coefficient ($ml\,g^{-1}$) |
| $K_F$ | Freundlich isotherm constant ($mg\,g^{-1}$) ($mg\,l^{-1}$)$^{-1/n}$ |
| $K_S$ | Sips isotherm constant ($l\,g^{-1}$) |
| $m_S$ | Sips isotherm exponent |
| $M$ | mass of the adsorbent (g) |
| $n$ | Freundlich isotherm exponent |
| $q_{cal}$ | calculated solid phase Pb(II) concentration at equilibrium ($mg\,g^{-1}$) |
| $q_{DR}$ | adsorption capacity of D–R isotherm ($mol\,g^{-1}$) |
| $q_e$ | amount of Pb(II) removed from aqueous solution at equilibrium ($mg\,g^{-1}$) |
| $q_{exp}$ | experimentally measured solid phase Pb(II) concentration at equilibrium ($mg\,g^{-1}$) |
| $q_{mL}$ | monolayer capacity of Langmuir equation ($mg\,g^{-1}$) |
| $q_{mS}$ | specific adsorption capacity of Sips equation at saturation ($mg\,g^{-1}$) |
| $q_S$ | specific adsorption capacity of Sips equation at saturation ($mg\,g^{-1}$) |
| $q_t$ | amount of Pb(II) adsorbed on the adsorbent surface at any time, $t$ ($mg\,g^{-1}$) |
| $R$ | universal gas constant ($8.314\,J\,K^{-1}\,mol^{-1}$) |
| $t$ | reaction time (min) |
| $T$ | absolute temperature (K) |
| $V$ | volume of solution (ml) |

*Greek symbols*

| | |
|---|---|
| $\beta$ | constant of D–R isotherm ($mol^2\,kJ^{-2}$) |
| $\varepsilon$ | Polanyi potential |

environmental remediation application of such nanostructured manganese oxides, have been not explored much.

As far as field applications are concerned, using any metal oxides including manganese oxide in powder form, especially in nanosize, has several engineering limitations: (i) difficulty in solid–liquid separation, (ii) low hydraulic conductivity, and (iii) leaching of nanoparticles along with the treated effluent. It is known that in aqueous solutions, the presence of other ions can cause aggregation of nanoparticles and thereby reduce the reactivity. This phenomenon of ion induced aggregation of nanoparticles in aqueous suspension may be prevented by anchoring the nanoparticles on suitable matrices. Natural cellulose fiber, an abundantly available, economical, renewable, and environment friendly material is gaining interest as a template because of its nanoporous surface features. It is also interesting as a filtering medium in water and wastewater treatment due to the potential synergistic properties that may arise from the combination of materials. This kind of hybrid materials shows the inherent properties of the fibers, in particular flexibility and strength, and also the high adsorption properties of the surface bonded nanoparticles. Recently, natural cellulose fibers have been used as a substrate for *in situ* synthesis of metal and metal oxide nanoparticles [16,17]. Nanostructure and the high oxygen density of cellulose fibers appear to form an effective nanoreactor, suitable for the *in situ* synthesis and stabilization of metal nanoparticles [18]. Alfaya and Gushikem [19] have studied aluminum oxide coated cellulose fibers modified with n-propylpyridinium chloride silsesquioxane polymer for the removal of $Fe^{3+}$, $Cu^{2+}$, and $Zn^{2+}$ from ethanol solutions. Fischer and Lieser [20] have synthesized cellulose exchangers carrying chelating anchor groups for selective separation of uranyl ions. Though limited reports are available on cellulose as a support for metal/metal oxide nanoparticles, to the best of our knowledge, no studies have been reported on the *in situ* synthesis of cellulose fiber supported nanoscale-manganese oxide and its application as a filter medium for scavenging heavy metals such as Pb(II).

In this paper, we explored the use of a novel cellulose-nanoscale-manganese oxide composite (C–NMOC) for removing Pb(II) ions from contaminated water. The performance of C–NMOC was compared with unsupported nanoscale-manganese oxide (NMO) prepared through a similar route. The studies report: (i) the synthesis and detailed characterization of NMO and C–NMOC, (ii) application of these materials for Pb(II) ions removal from aqueous medium, and (iii) spectroscopic and microscopic studies to probe the mechanism of Pb(II) removal by NMO and C–NMOC.

## 2. Materials and methods

### 2.1. Chemicals

Chemicals used in this study were of analytical grade. Potassium permanganate and ethyl alcohol were procured from Merck Limited, India and Jiangsu Huaxi International Trade Co. Ltd., China, respectively. Stock solution of 1000 $mg\,l^{-1}$ of Pb(II) was prepared from lead nitrate $Pb(NO_3)_2$ using distilled water. Required concentrations of the samples were prepared by serial dilutions of the stock solution. Standard Pb(II) solution of 1000 $mg\,l^{-1}$ for atomic absorption spectroscopy (AAS) was procured from SRL Chemicals, India.

### 2.2. Synthesis of adsorbents

C–NMOC composites were prepared by impregnating $KMnO_4$ solution into cellulose fiber matrix (Lenzis AG, India) for 30 min. $KMnO_4$ impregnated cellulose fibers were subsequently reduced by adding ethanol drop by drop under stirring. Stirring continued for 15 min and the reaction mixture was kept at rest for two hours. The cellulose fibers changed their colour from golden brown to brownish black with increasing manganese loading from 0.39 to 4.64%, which indicates the formation of manganese oxide on the cellulose fiber matrix. The concentration of manganese oxide loadings on cellulose was varied by changing the molar concentrations of $KMnO_4$ from 0.025 to 0.1 M. The composites specimens were then washed with deionised water and dried at $60 \pm 1\,^{\circ}C$ for 24 h and stored in an air tight polythene cover for further use. The as-prepared samples were labeled as C–NMOC(A), C–NMOC(B), C–NMOC(C), and C–NMOC(D), in increasing order of manganese loading.

NMO was synthesized by chemical reduction of $KMnO_4$ by ethanol, similar to a procedure described by Subramanian et al. [15]. In a typical synthesis, a known amount of $KMnO_4$ was initially dissolved in deionised water. Subsequently, ethanol was added drop by drop under stirring (15 min). The solution was kept at rest for two hours and the brown colored precipitate obtained was filtered and washed thoroughly with deionised water. The product was dried at $60 \pm 1\,^{\circ}C$ for 24 h, ground well and stored in an air tight container for further use.

### 2.3. Material characterization

The phase(s) present in the as-synthesized NMO, C-NMO and Pb(II) adsorbed materials were determined via X-ray diffractometry (Bruker AXS, D8 Discover, USA) using Cu Kα radiation at $\lambda = 1.5418$ Å, operated at 35 kV and 25 mA. A scan step of 1 s and

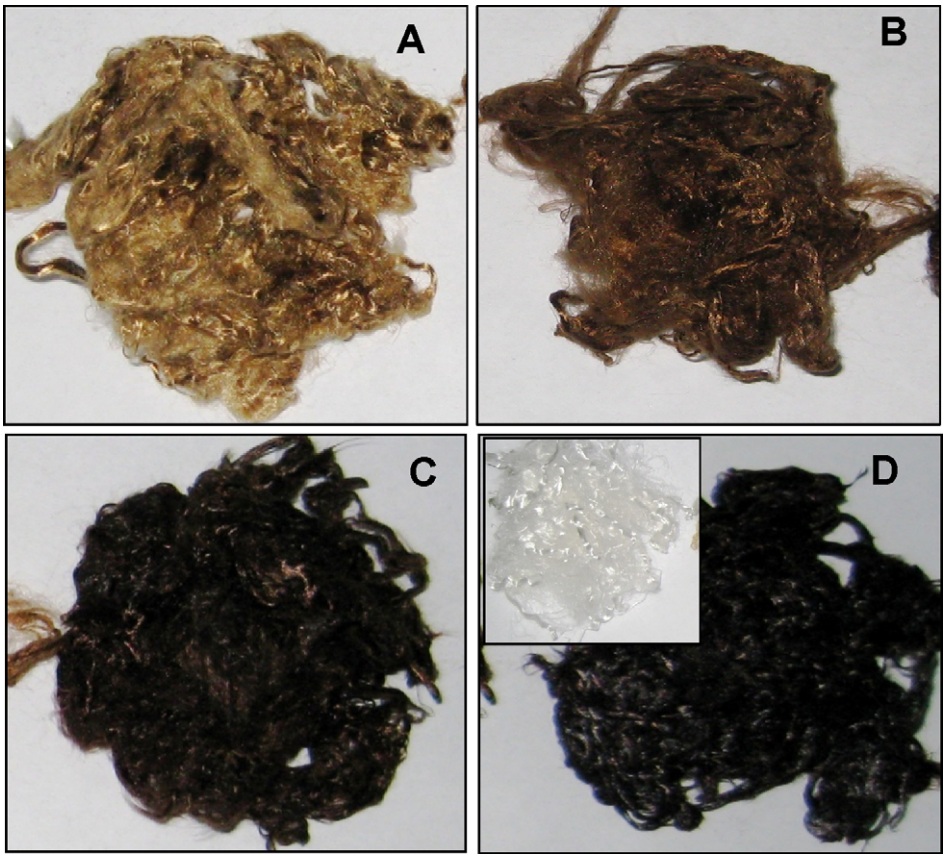


**Fig. 1.** Photographs of manganese oxide loaded cellulose fibers (C–NMOC). Various loadings of Mn on cellulose fibers (A) 0.39% Mn, (B) 0.66% Mn, (C) 3.7% Mn and (D) 4.64% Mn. Pristine cellulose fibers are shown in inset of panel 'D'.

step size ($2\theta$) of 0.1° was applied to record the patterns in the range from 10 to 90° ($2\theta$). Surface morphology, elemental analysis and elemental mapping studies were carried out using scanning electron microscopy (SEM) equipped with energy dispersive analysis of X-rays (EDAX) (FEI Quanta 200, Czechoslovakia). High resolution transmission electron microscopy (HRTEM) images of the samples were obtained with JEM 3010 with a UHR polar piece (JEOL, Japan). X-ray photoelectron spectroscopic (XPS) analysis was done using ESCA Probe TPD of Omicron Nanotechnology. Polychromatic Mg Kα was used as the X-ray source ($h\nu$ = 1253.6 eV). Spectra in the required binding energy range were collected and an average was taken. Beam induced damage of the sample was reduced by adjusting the X-ray flux. Binding energy was corrected with respect to C 1s at 285.0 eV. Manganese loading in the C–NMOC was quantified by acid digestion method suggested by the National Environment Protection Council [21]. Fourier transform infrared (FT-IR) spectra were collected (450–4000 $cm^{-1}$) using PerkinElmer Spectrum One FT-IR spectrometer, USA.

### 2.4. Lead(II) uptake studies

All the adsorption studies were carried out in 250 ml conical flasks. The working volume of the Pb(II) solution was taken as 100 ml and required dose of the as-synthesized adsorbents were added. Immediately after the addition of the adsorbents, the flasks were shaken at 160 ± 5 rpm in an orbital shaker (Rivera, India) at 30 ± 2 °C. Samples were withdrawn at predetermined time intervals and residual Pb(II) concentrations were measured using an atomic absorption spectrophotometer (AAnalyst 700, PerkinElmer, USA). Time dependent adsorption studies were done at two different Pb(II) concentrations of 50 and 100 mg $l^{-1}$. Isotherm studies were performed by varying the concentrations of the Pb(II) solution over a wide range (50–500 mg $l^{-1}$). Effects of adsorbent dose and ionic strength were investigated at a pH of 5 ± 0.2 and Pb(II) concentration of 100 mg $l^{-1}$. Effect of pH on Pb(II) adsorption was also carried out by varying the pH from around 2.5–5.5 and pH above 5.5 were not tried to avoid any possible precipitation of lead hydroxide [6]. The pH of the samples were adjusted using dilute NaOH or HCl solutions.

### 2.5. Regeneration studies

The reusability of any used adsorbent mainly depends on the ease with which the adsorbed solute desorbs from the spent adsorbent. In this study, the reuse potential of the Pb(II) adsorbed C–NMOC was tested. Initially, 100 mg $l^{-1}$ of Pb(II) was adsorbed onto C–NMOC. After attaining equilibrium, the Pb(II) loaded adsorbents were separated from the solutions carefully and immersed in 100 mL of various concentrations of HCl (0.05–0.3 M) for 30 min. All other conditions were maintained as above. The concentration of the solute leached into the elutant was estimated as described earlier. In order to check the reusability of the regenerated adsorbents, 3 cycles of consecutive adsorption–desorption studies were performed.

## 3. Results and discussion

### 3.1. Material characterization

#### 3.1.1. Quantification of manganese loading in C–NMOC

Manganese loading on C–NMOC was quantified by acid digestion method. For this, 1 g of C–NMOC was dissolved in aqua regia similar to a procedure described by NEPC [21]. Fig. 1 (panels A–D) shows the photographs of C–NMOC loaded with different amounts

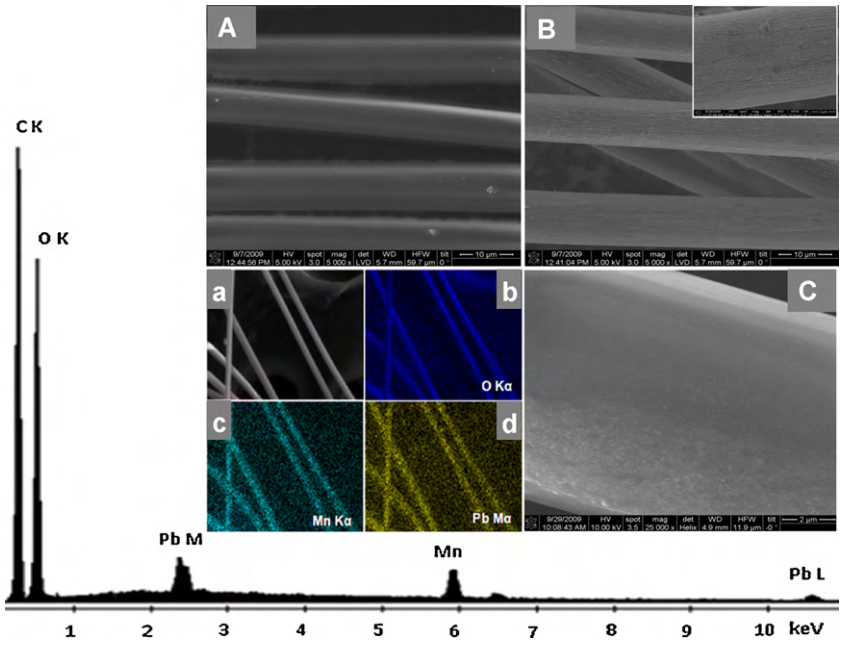


**Fig. 2.** EDAX spectrum of C–NMOC (4.64% Mn loading) after Pb(II) adsorption. Inset: elemental X-ray images of O Kα (b), Mn Kα (c), and Pb Mα (d) of the sample. The corresponding SEM image is shown in (a). FESEM micrographs of pristine cellulose (A), 4.64% Mn loaded C–NMOC (B), and 0.39% Mn loaded C–NMOC (C). Inset of panel 'B' shows FESEM image of Pb(II) adsorbed C–NMOC (4.64% Mn loading).

of manganese oxide. The color of C–NMOC changed from golden brown to brownish black upon increasing manganese loading from 0.39 to 4.64%. Various Mn loaded C–NMOC are labeled with suffixes A, B, C and D with an increasing order of Mn loading. The C–NMOC samples A, B, C and D contain 0.39%, 0.66%, 3.7% and 4.64% Mn, respectively.

### 3.1.2. Microscopic analysis

FESEM micrographs of C–NMOC before and after Pb(II) adsorption are shown in inset of Fig. 2 (panel A–C). Unless otherwise mentioned, 4.64% Mn loaded C–NMOC sample was used for all Pb(II) uptake studies. The images show that cellulose fibers are cylindrical in shape with uniform dimensions (9.5–9.8 μm). At lower Mn loading (0.39% Mn loading) (Fig. 2C), well dispersed manganese oxide particles are seen on the cellulose surface. Particle size appears too small for observation under FESEM. At higher Mn loading, the entire surface is modified and uniform coating is formed. EDAX analysis confirms the presence of Mn, O and Pb on the C–NMOC surface and uniform distribution of these elements (Fig. 2). The SEM micrographs of as synthesized NMO and Pb(II) reacted NMO are shown in Fig. S1 of supplementary data. From these images, it can be seen that NMO powders are agglomerated nanoparticles and they lose the nanoscale features and become bigger size particles after Pb(II) adsorption. The EDAX spectrum and the elemental imaging confirm the presence of adsorbed Pb(II) on the NMO surface (Fig. S2 of supplementary data). Fig. S3 of supplementary data show the HRTEM micrographs of NMO particles. These images confirm that particles are agglomerated whiskers in nanoscale and the particle size varies from 5 to 10 nm. A selected-area electron diffraction (SAED) pattern of NMO is shown in Fig. S3 of supplementary data. This reveals the nanocrystalline nature of the material, which is consistent with the XRD observation.

### 3.1.3. X-ray photoelectron spectroscopic analysis

The XPS survey spectra of C–NMOC(D) before and after Pb(II) adsorption are given in Fig. 3A. The corresponding spectra for NMO are shown in Fig. S4 (panel A) of supplementary data. These photoelectron peaks further confirm the existence of adsorbed Pb along with the principal elements Mn and O in NMO and C–NMOC. The presence of small amounts of carbon on NMO surface is due to surface contaminants. For further analysis of the chemical form of adsorbate and adsorbent before and after exposure to Pb(II) ions, detailed scans of Mn, O and Pb regions were performed. The XPS spectrum of Mn 2p region in NMO shows the Mn $2p_{3/2}$ feature at 642.7 eV with a separation of 11.7 eV from Mn $2p_{1/2}$, which is agreement with Mn(IV) in $MnO_2$ [22]. The XPS spectrum of Mn 2p after the adsorption of Pb(II) shows no shift and the binding energies match exactly with those of Mn $2p_{3/2}$ and $2p_{1/2}$ of pristine NMO (Fig. S4 (panel B) of supplementary data). The deconvoluted spectrum of O 1s shows peaks at 530.2, 531.6 and 532.8 eV (Fig. S4 (panel C) of supplementary data). The low binding energy peak at 530.2 eV can be assigned to lattice oxygen in the form of $O^{2-}$ (characteristic of the oxygen in manganese oxides) [22]. The peak at 531.8 eV can be assigned to surface adsorbed oxygen in the form of $OH^-$ and the highest energy peak can be attributed to adsorbed $H_2O$. As in the case of Mn 2p, no shift in O 1s peaks was observed after Pb(II) adsorption (data not shown). The XPS spectrum of Pb in Pb(II) adsorbed NMO shows the doublet peaks at 138.4 eV (Pb $4f_{7/2}$) and 143.2 eV (Pb $4f_{5/2}$) (Fig. S4 (panel D) of supplementary data). The peak observed at 138.4 eV can be assigned to PbO [23,24]. This shows a fixation of Pb(II) onto NMO. XPS data support no evidence for the oxidation of Pb(II) to Pb(IV) nor the formation of new solid phases, which is consistent with the XRD data.

Detailed photoelectron spectra of Mn 2p, O 1s and Pb 4f in C–NMOC(D) and Pb(II) adsorbed C–NMOC(D) are shown in Fig. 3B–D, respectively. From the data, it is clear that there is a 1.5 eV shift in Mn $2p_{3/2}$ (641.2 eV) compared to NMO. The shift in Mn 2p peak towards the lower binding energy clearly indicates that cellulose plays a role in the oxidation state of manganese in C–NMOC. Even though a scatter in binding energies of Mn 2p can be observed in the litterateur, a decrease in binding energy generally points towards a decrease in the oxidation state. According to literature, Mn $2p_{3/2}$ binding energy value of 641.2 may be ascribed to $Mn_2O_3$ [25]. The decrease in binding energy could be attributed to the effect of the support. Radhakrishnan and Oyama [26] reported that the support influences the morphology, the electronic state, and

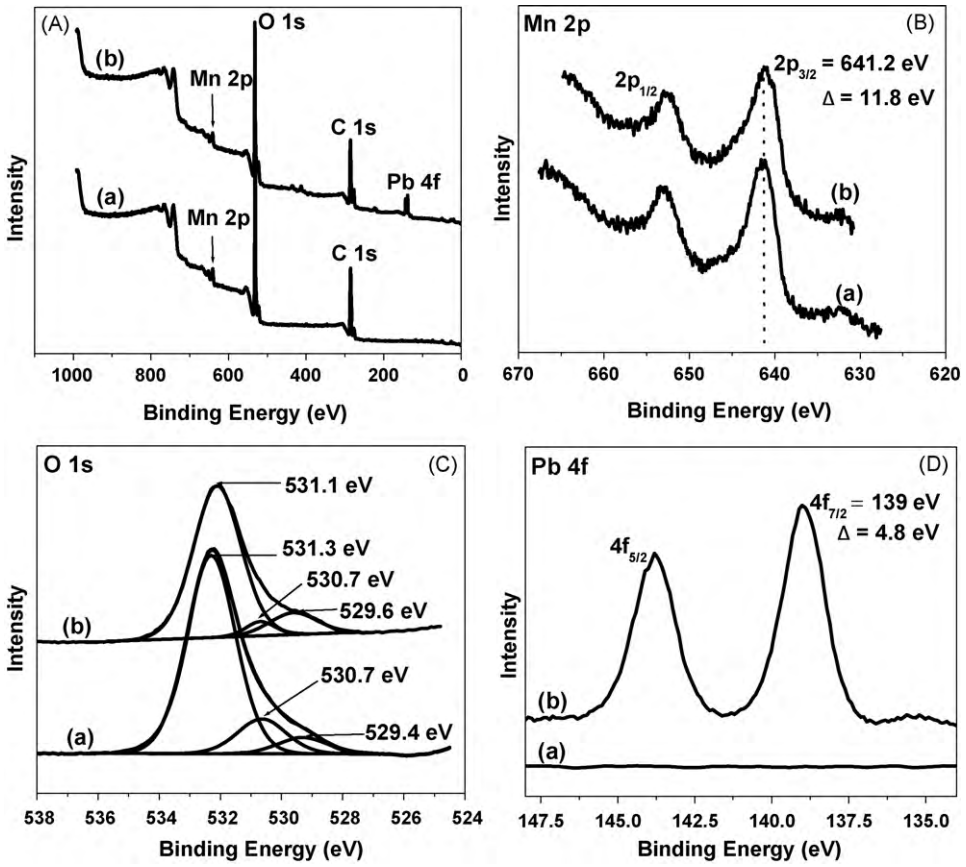


**Fig. 3.** X-ray photoelectron spectra of C–NMOC (4.64% Mn loading) (a) before and (b) after Pb(II) adsorption. (A) Survey spectra and (B–D) spectra of various regions. The traces are shifted vertically for clarity.

the catalytic activity of manganese oxide particles. They reported a lower energy shift in the positions of the $L_{II}$ and $L_{III}$ Mn L-edge features observed through near-edge X-ray absorption fine structure (NEXAFS) analysis. They also observed a variation in $L_{III}/L_{II}$ intensity ratio for $MnO_x$ dispersed on various supports. These observations clearly indicate that support plays a role in oxidation state of Mn in $MnO_x$ and the nature of the Mn active site on the surface.

As observed in the case of NMO, the O 1s peak in C–NMOC(D) did not show significant variation before and after Pb(II) adsorption. The low binding energy peak observed at 529.4 eV can be ascribed to be characteristic of oxygen in manganese oxide of C–NMOC(D). The intermediate binding energy peak can be ascribed to surface adsorbed $OH^-$ and the highest energy peak can be largely due to characteristic oxygen in cellulose. Similar O 1s photoelectron peaks were observed, even after adsorption of Pb(II). However, the peak observed at lower binding energy (529.6 eV) can be ascribed to oxygen in lead oxide and manganese oxides. The peak observed at 139 eV (Pb $4f_{7/2}$) shows the fixation of Pb(II) onto C–NMOC(D) and the peak can be ascribed to PbO [22]. XPS data does not support the oxidation of Pb(II) to Pb(IV), nor the formation of new solid phases.

### 3.1.4. X-ray diffraction analysis

The XRD patterns of C–NMOC(D) and NMO before and after Pb(II) adsorption are shown in Fig. S5 of supplementary data. The XRD patterns of C–NMOC(D) and Pb(II) adsorbed C–NMOC(D) have no visible changes as such. C–NMOC showed a broad peak at $2\theta = 21.7^\circ$, which can be ascribed to the high intensity (0 0 2) plane of cellulose. A weak peak at $2\theta = 12.2^\circ$ is also observed. These diffraction angles are characteristic of cellulose II crystal structure [27]. No visible crystalline peaks corresponding to manganese oxide was observed even at a manganese loading of 4.64%, this may be attributed to small crystallite size, which is apparently below the detection limit of XRD or may be due to amorphous nature of the manganese oxide prepared. X-ray patterns of NMO exhibited broad peaks corresponding to (0 0 2), (1 0 0) and (1 1 0) planes. These planes can be ascribed to poorly crystalline layered birnessite structure [13,14]. The additional peak appeared in Pb(II) adsorbed NMO can be attributed to the (1 1 1) plane of PbO. An increase in particle size was also evident from the decrease in width of the peaks of Pb(II) adsorbed NMO. The relative sharpening of the peaks can be attributed to the ion induced aggregation of manganese oxide nanoparticles during Pb(II) adsorption.

### 3.1.5. Infrared spectroscopic analysis

Infrared spectroscopy was used to study the interaction of the metal oxide with the support and the interaction of composites with Pb(II). Fig. 4 shows the FT-IR spectra of cellulose (a), C–NMOC(D) before (b) and after (c) Pb(II) ions adsorption. The IR band located at 1421 $cm^{-1}$ can be assigned to the $CH_2$ scissoring motion and IR band at 896 $cm^{-1}$ can be assigned to C–O–C stretching at the β-(1 → 4)-glycosidic linkage. The features of these two bands are typical of type II crystalline (cellulose II) and amorphous cellulose [27]. Absence of changes in the IR bands at 1421 $cm^{-1}$ and 896 $cm^{-1}$ also suggests that incorporation of manganese oxide and adsorption of Pb(II) onto cellulose did not modify the initial structure of cellulose. IR spectrum of NMO shows bands at 520 and 720 $cm^{-1}$ and it is attributed to the stretching vibration of Mn–O and Mn–O–Mn bonds in layered birnessite [28]. The IR spectrum of the Pb(II) adsorbed NMO did not show any changes in the band positions. This indicates that no chemical modification has happened to NMO after Pb(II) adsorption (data not shown).

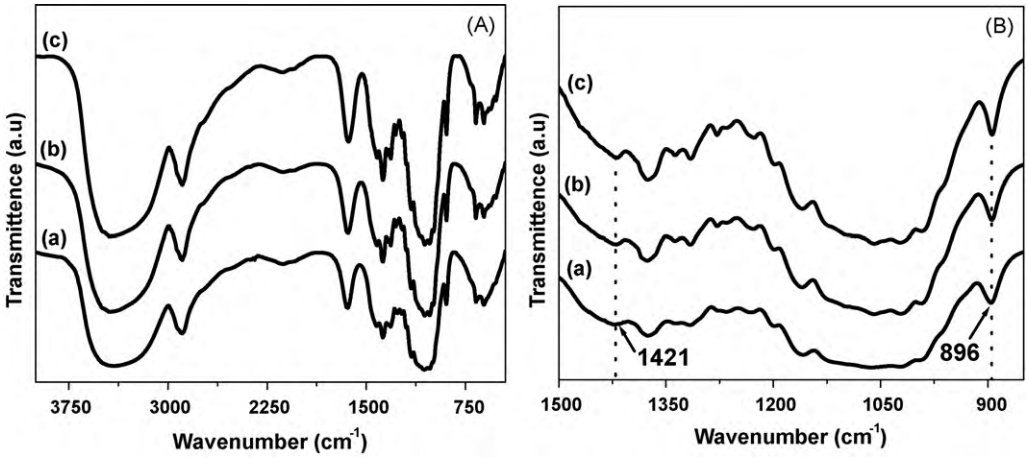


**Fig. 4.** FT-IR spectra of (a) cellulose and C–NMOC (4.64% Mn loading) (b) before and (c) after Pb(II) adsorption. A and B correspond to the total spectrum and an expanded view of the 850–1500 $cm^{-1}$ spectral region, respectively. The traces are shifted vertically for clarity.

### 3.2. Lead(II) removal studies

#### 3.2.1. Effect of adsorbent dose

Pb(II) adsorption by C–NMOC (A, B, C and D) and NMO as a function of adsorbent dose were studied and the results are shown in Fig. 5A. Studies were also performed with bulk manganese oxide (BMO) and unmodified cellulose fibers as well. As expected, the amount of Pb(II) adsorption increased with increase in adsorbent dose. Increased Pb(II) removal with increase in dose can be attributed to the availability of more and more binding sites for Pb adsorption. The results also show that incorporation of manganese oxide onto cellulose fibrous matrix enhanced its Pb(II) adsorption capacity significantly. A direct relationship between manganese oxide loading in C–NMOC and Pb adsorption capacity was observed. On the other hand, the plots of unit equilibrium adsorption capacity ($q_e$) versus quantity of manganese oxide in C–NMOC revealed that the $q_e$ was significantly high at low manganese oxide loading and reduced upon increasing the manganese oxide loading on C–NMOC (Fig. 5B). These can be attributed to better dispersion of manganese oxide at lower loading. Generally, an adsorbent concentration effect, i.e., a decrease in equilibrium uptake with increase in the adsorbent dose, was observed with all the adsorbents tested. This is mainly because of unsaturation of adsorption sites resulting from the lower adsorptive capacity utilization of the adsorbent during the adsorption process. It is also worth to note that a significant improvement in unit uptake capacity (per gram of Mn) was observed for manganese oxide prepared on the cellulose fiber compared to pristine NMO. The enhanced Pb(II) uptake may be due to the well dispersed nature of the supported $MnO_x$ and reduced interparticle collision and thereby reduced aggregation. Since, CNMOC(D) has shown maximum Pb(II) uptake capacity per gram of material, further studies were restricted to C–NMOC(D) alone. Now onwards, C–NMOC(D) is represented as C–NMOC.

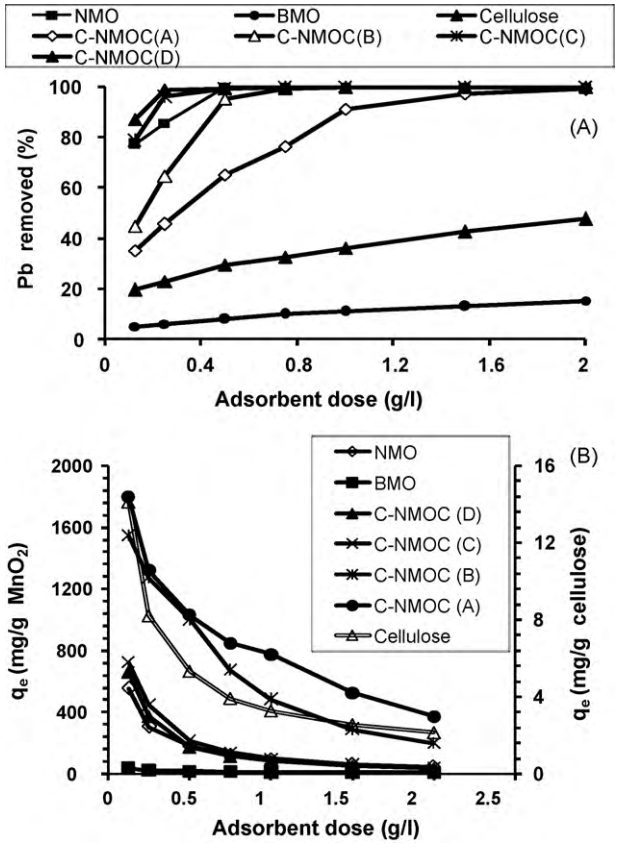


**Fig. 5.** Effect of adsorbent dose on Pb(II) removal by various adsorbents. % Pb(II) removal as a function of adsorbent dose (A), unit Pb(II) uptake capacity as a function of manganese content in each adsorbent (B). *X*-axis scale for cellulose and C–NMOC = 10×; *X*-axis scale for NMO and BMO = 1×.

#### 3.2.2. Effect of pH

Influence of pH on Pb(II) adsorption by C-MNOC and NMO was investigated and the data are shown in Fig. 6. It is clear from the figure that Pb(II) adsorption by C–NMOC is less sensitive to pH variations compared to NMO. Optimum removal of Pb(II) by NMO was achieved at pH 5 whereas C–NMOC removed more than 90% of the Pb(II) even at an initial pH of 2.5.

In order to better assess the Pb(II) binding ability of adsorbents at various pH, the coefficient of distribution ($K_d$) value was plotted as a function of pH (Fig. 6). The $K_d$ values were calculated using the following mathematical expression.

$$K_d = \left(\frac{C_i - C_e}{C_e}\right)\left(\frac{V}{M}\right) \quad (1)$$

It is reported that higher the $K_d$ value, better is the binding ability of the target pollutant. In general, the $K_d$ values in the range of $10^3$ ml $g^{-1}$ are considered good, and those above $10^4$ ml $g^{-1}$ are outstanding [29]. From the results it is clear that both NMO and C–NMOC are outstanding adsorbents in removing Pb(II) ions from aqueous solution. However, the Pb(II) binding ability of C–NMOC is superior to NMO at lower pH values (pH < 4). It is also worth to note that $K_d$ vs pH plots of NMO sharply increases with increase in

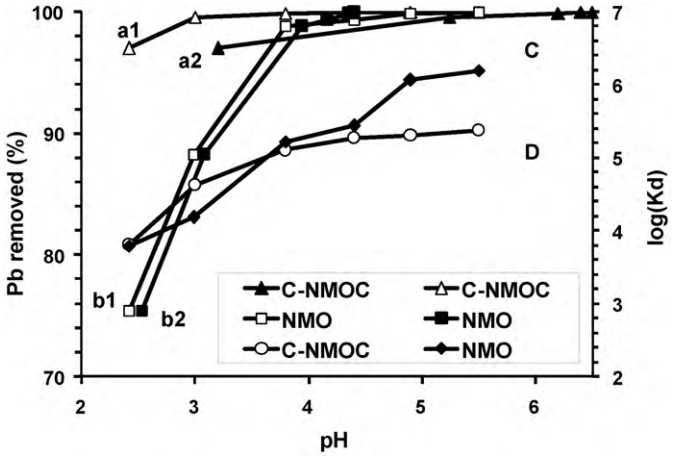


**Fig. 6.** Effect of pH on Pb(II) adsorption by NMO and C–NMOC (4.64% Mn loading). a1, b1, C, and D are plotted against initial pH; a2 and b2 are plotted against pH at equilibrium uptake capacity; C and D plots represent log($K_d$) value at various pHs.

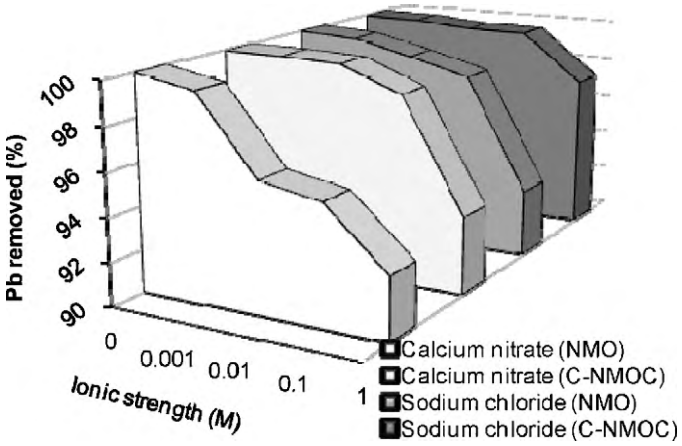


**Fig. 7.** Effect of ionic strength on Pb(II) adsorption by NMO and C–NMOC (4.64% Mn loading).

pH whereas it is relatively flat in the case of C–NMOC, indicating less sensitive nature of C–NMOC to pH.

Apart from the effect of pH on the extent of adsorption, it can also alter the solubility of the target metal. Hence, it is important to know that Pb(II) removal at a particular pH has happened through lead hydroxide formation or adsorption of divalent lead ion. Following equations are used to calculate the pH at which lead hydroxide starts to form [30].

$$Pb(OH)_2 \leftrightarrow Pb^{2+} + 2OH^- \quad (2)$$

$$pH = 14 - \log\left[\frac{\sqrt{Pb^{2+}}}{\sqrt{K_{sp}}}\right] \quad (3)$$

$$K_{sp} = [Pb^{2+}][OH^-]^2 \quad (4)$$

where $K_{sp}$ is the solubility product of lead hydroxide ($[Pb^{2+}][OH^-]^2$) and its value at 25 °C is $1 \times 10^{-16}$ [31] and the initial Pb(II) concentration used was around 100 mg $l^{-1}$ (0.483 mM), hence the pH at which $Pb(OH)_2$ starts forming is about 7.7. Therefore, the solution phase formation of $Pb(OH)_2$ as the reason for Pb(II) removal can be ruled out since initial pH of the solution was kept below 5.5.

### 3.2.3. *Effect of ionic strength*

The background salts may complex with oxide metals and compete for adsorption sites. Hence, it is important to know the effect of ionic strength on the adsorption of metal ions on oxide surfaces. Ionic strength was tested by the addition of sodium chloride and calcium nitrate to the solution of Pb(II) and the results are shown in Fig. 7. Experimental data reveal that Pb(II) uptake capacity of NMO and C–NMOC decreased with increase in ionic strength. This decrease in binding affinity of Pb(II) with increase in ionic strength could be attributed to the competitive effect of background ions such as $Na^+$ and $Ca^{2+}$ for the Pb(II) adsorption sites. The other reason one could attribute to the decreased uptake capacity is due to the interaction between the positive metal ions with the anions present in the background electrolyte and the formation of corresponding Pb(II) salts. This can cause decrease in effective concentration of free Pb(II) ions and hence uptake capacity. It is also known that at higher ionic strength, the activity of metal ions in solution decreases due to increasing non-ideality of solution, and hence reducing uptake. This increase in non-ideality is due to increasing electrostatic interaction and results in the formation of ion pair [32]. Experimental evidence also reveals that the addition of $Ca^{2+}$ ions has predominant effect on Pb(II) uptake compared to $Na^+$. This may be attributed to higher positive charge of $Ca^{2+}$ and hence higher competition for the binding sites [24]. From the Fig. 7, it can also be seen that NMO has greater influence on ionic strength compared to C–NMOC. This can be attributed to ion induced aggregation of NMO particles and hence reduced reactivity. However, the possibility of such aggregation can be less in C–NMOC due to less interparticle collision. Even though some reduction in Pb(II) removal by C–NMOC was observed with increase in salt concentrations, a significant amount of Pb(II) removal was obserevd even at high background ionic strength (0.1 M). Hence, one may be able to use such a system for removing Pb(II) from water containing common salt, particularly with higher amount of Pb(II).

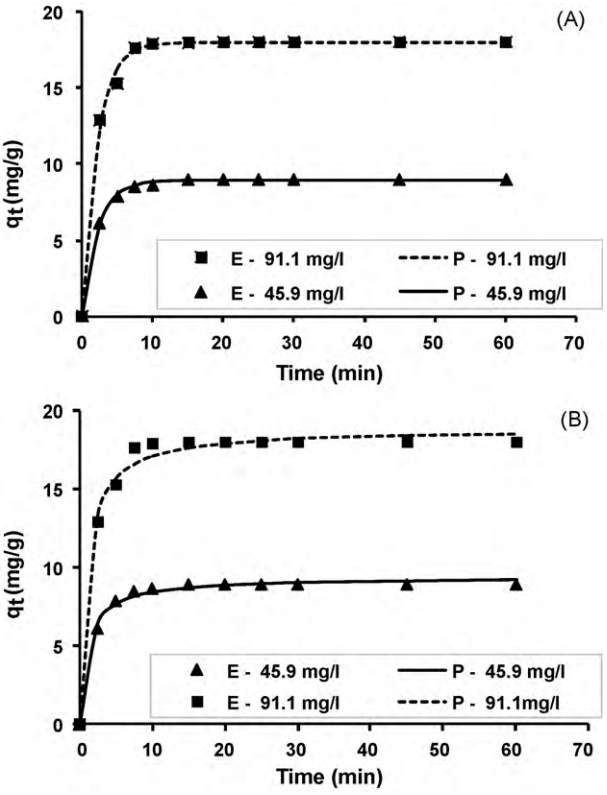


**Fig. 8.** Comparison of pseudo-first-order (A) and pseudo-second-order (B) kinetic plots with experimental data for adsorption of Pb(II) by C–NMOC (4.64% Mn loading). E: experimental; P: predicted.

**Table 1**
Pseudo-first-order and pseudo-second-order rate parameters obtained for the adsorption of Pb(II) by C–NMOC (4.64% Mn loading) and NMO.

| Adsorbents | Pb conc. ($mg\,l^{-1}$) | Pseudo-first-order-rate parameters | | | | Pseudo-second-order-rate parameters | | | |
|---|---|---|---|---|---|---|---|---|---|
| | | $k_1$ ($min^{-1}$) | $q_e$ ($mg\,g^{-1}$) | RMSE | $\chi^2$ | $k_2$ ($g\,mg^{-1}\,min^{-1}$) | $q_e$ ($mg\,g^{-1}$) | RMSE | $\chi^2$ |
| C–NMOC | 45.9 | 0.45 | 8.88 | 0.099 | 0.009 | 0.098 | 9.35 | 0.242 | 0.048 |
| | 91.1 | 0.47 | 17.93 | 0.384 | 0.077 | 0.053 | 18.80 | 0.519 | 0.133 |
| NMO | 45.9 | 0.43 | 91.43 | 2.230 | 0.288 | 0.005 | 96.62 | 3.610 | 0.760 |
| | 91.1 | 0.46 | 180.72 | 1.170 | 0.150 | 0.009 | 190.5 | 2.690 | 0.702 |

### 3.2.4. Kinetics of adsorption

The effects of contact time and initial Pb(II) concentrations were investigated in this study. The kinetics of Pb(II) uptake capacity of C–NMOC at various initial concentrations of Pb(II) is shown in Fig. 8. The corresponding data for NMO is shown in Fig. S6 of supplementary data. From these figures, it is apparent that adsorption of Pb(II) onto NMO and C–NMOC is a fast process and most of the adsorption happened in a short period (<10 min) and the system achieved pseudo equilibrium at 60 min of contact time from the commencement of the adsorption process. Rapid adsorption compared to bulk particles may be attributed to relatively large surface area, greater density of reactive sites on the particle surfaces, and/or higher intrinsic reactivity of the surface sites [33].

To understand the process better, experimental kinetic data of Pb(II) adsorption by NMO and C–NMOC were analysed with various reaction kinetic models including Lagergren pseudo-first-order [34,35] and Ho's pseudo-second-order [36] reaction rate models. Mathematical representations of these models are given in Eqs. (5) and (6).

$$\text{Pseudo-first-order equation}: \; q_t = q_e(1 - e^{-K_1 t}) \tag{5}$$

$$\text{Pseudo-second-order equation}: \; q_t = \frac{q_e^2 k_2 t}{1 + q_e k_2 t} \tag{6}$$

A non-linear approach was used to find the best-fitting model and kinetic parameters, which were found by trial and error method by means of Microsoft's spreadsheet, Excel® software package using solver add-in option [37]. The simulated plots along with experimental ones for C–NMOC are depicted in Fig. 8. The corresponding data for NMO are given in Fig. S6 of supplementary data. Comparing the experimental and model predicted kinetic profiles, we see that both the models have described the kinetic data fairly well. However, the model predicted kinetic parameters and their associated error measurements show (Table 1) that pseudo-first-order equation is more appropriate in predicting the experimental data.

### 3.2.5. Adsorption equilibrium

An accurate mathematical description of equilibrium adsorption capacities is indispensable for reliable predictive modeling of adsorption systems. Several adsorption isotherm models, including two, three and four parameter models, have been introduced over the years, for these purposes. However, each model has its own limitations because of the underlying assumptions involved in their respective derivation. No single model developed so far is applicable generally for describing the adsorption contact process [38]. A particular isotherm may fit the experimental data accurately under one set of conditions, but may fail entirely under another set of conditions. Some of the important isotherm models reported in the literature that can explain solid–liquid equilibrium are: Langmuir (L), Freundlich (F), and Sips (S). Table 2 gives the mathematical representations of the isotherm models. More details of these models are available elsewhere [38,39].

**Table 2**
Two and three parameter isotherm models.

| Model | Mathematical expressions | Model parameters |
|---|---|---|
| Langmuir | $q_e = \frac{q_{mL} b_L C_e}{1 + b_L C_e}$ | $q_{mL}$ ($mg\,g^{-1}$), $b_L$ ($l\,mg^{-1}$) |
| Freundlich | $q_e = K_F C_e^{1/n_F}$ | $K_F$ ($mg\,g^{-1}$) ($mg\,l^{-1}$)$^{-1/n}$, $n_F$ |
| Sips | $q_e = \frac{q_{mS}(K_S C_e)^{m_S}}{1 + (K_S C_e)^{m_S}}$ | $K_S$ ($l\,mg^{-1}$), $q_{mS}$ ($mg\,g^{-1}$), $m_S$ |

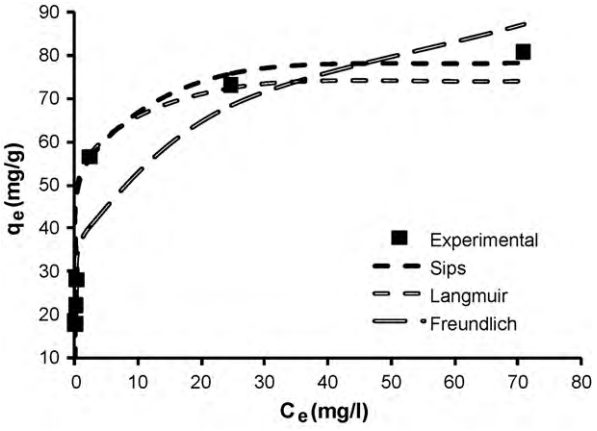


**Fig. 9.** Two and three parameter isotherm model plots for the adsorption of Pb(II) onto C–NMOC (4.64% Mn loading).

Fig. 9 shows various isotherms plots obtained for the adsorption of Pb(II) by C–NMOC. The corresponding figure for NMO is given in Fig. S7 of supplementary data. The estimated isotherm parameters from these model fits are given in Table 3. The classical L and F models (two parameter models) showed poor correlation with the experimental data compared to three parameter models. All the 'three-parameter' models tested were able to predict the adsorption onto both NMO and C–NMOC fairly well, which is evident from

**Table 3**
Isotherm parameters obtained for the adsorption of Pb(II) by C–NMOC (4.64% Mn loading) and NMO from fitting experimental equilibrium data with various isotherm models.

| Isotherm models | Model parameters | Estimated model parameters | |
|---|---|---|---|
| | | NMO | C–NMOC |
| Freundlich | $K_F$ ($mg\,g^{-1}$) ($mg\,l^{-1}$)$^{-1/n}$ | 207.39 | 32.6 |
| | $n$ | 9.20 | 4.33 |
| | RMSE | 25.59 | 8.28 |
| | $\chi^2$ | 23.61 | 15.13 |
| Langmuir | $q_{mL}$ ($mg\,g^{-1}$) | 326.74 | 75.04 |
| | $b_L$ ($l\,mg^{-1}$) | 10.80 | 1.25 |
| | RMSE | 25.65 | 2.50 |
| | $\chi^2$ | 30.10 | 0.60 |
| Sips | $q_{mS}$ ($mg\,g^{-1}$) | 395.77 | 80.10 |
| | $K_S$ ($l\,g^{-1}$) | 2.25 | 1.02 |
| | $m_S$ | 0.35 | 0.89 |
| | RMSE | 9.96 | 1.49 |
| | $\chi^2$ | 3.45 | 0.33 |
| Dubinin–Radushkevich | $q_{DR}$ ($mol\,g^{-1}$) | 314.19 | 35.85 |
| | $\beta$ ($mol^2\,kJ^{-2}$) | 0.01 | 0.06 |
| | $E_{DR}$ ($kJ\,mol^{-1}$) | 6.20 | 2.89 |

the low RMSE and Chi-square ($\chi^2$) values. Among the three parameter models tested, S isotherm predicted the data more closely and accurately for C–NMOC and the predicted uptake capacity was found to be 80.10 mg g$^{-1}$. The experimental evidence shows that the unsupported NMO is having Pb(II) uptake capacity in excess of 370 mg g$^{-1}$. The uptake capacity figures show that the as-prepared nanoadsorbents (C–NMOC and NMO) are superior in scavenging Pb(II) from aqueous medium in comparison to many media (supported and unsupported) investigated recently [5,40–43].

### 3.3. Free energy of adsorption

Dubinin–Radushkevich (D–R) isotherm can be used to find the free energy of adsorptions and hence the adsorption mechanism [44]. The mean free energy of adsorption ($E_{DR}$), defined as free energy change when 1 mol of ion is transferred from infinity in solution to the surface of the solid, can be estimated using the Eqs. (7)–(9).

$$E_{DR} = \frac{1}{(2\beta^{1/2})} \tag{7}$$

$$\ln q_e = \ln q_{DR} - \beta\varepsilon^2 \tag{8}$$

$$\varepsilon = RT \ln\left(1 + \frac{1}{C_e}\right) \tag{9}$$

A straight line plot of $\ln(q_e)$ vs $\varepsilon^2$ shown in Fig. S8 of supplementary data can be used to find $\beta$ and hence the mean free energy of adsorption. The values of $E_{DR}$ found in this study were 2.9 kJ mol$^{-1}$ for C–NMOC and 6.2 kJ mol$^{-1}$ for NMO, suggesting that electrostatic force plays dominant role in the adsorption process [45].

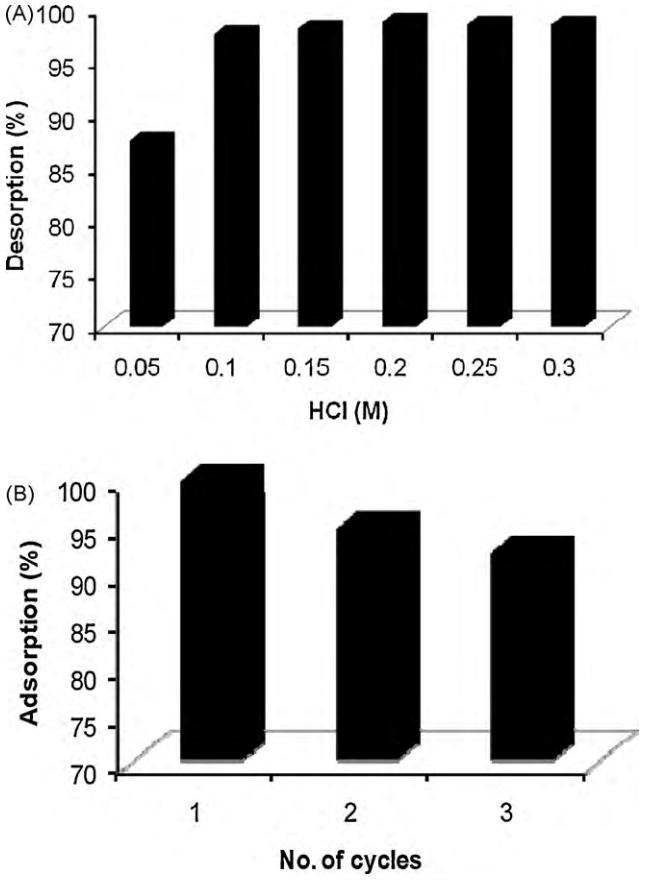


**Fig. 10.** Regeneration of spent C-NOMC by acid treatment. (A) Effect of acid concentration on Pb(II) desorption, (B) Pb(II) uptake (%) by C–NMOC in three consecutive cycles of adsorption process.

### 3.4. Regeneration

Adsorption process is more economically viable if the adsorbent can be regenerated and reused in many cycles of operation. This study aimed at developing a proper regeneration protocol for spent C–NMOC. The results show that an optimum HCl concentration of 0.1 M could elute more than 98% of the adsorbed Pb(II). No significant variation in Pb(II) desorption was observed above 0.1 M HCl (Fig. 10A). For checking the reuse potential of the adsorbent, successive adsorption–desorption cycles were conducted. The data reveals that C–NMOC has good reuse potential and no significant reduction in adsorption can be seen with repeated use. At the end of third cycle, the adsorption efficiency was reduced only <10% (Fig. 10B).

## 4. Conclusions

A novel hybrid adsorbent, C–NMOC was synthesized through a simple soft chemistry route. The synthesis process involves only one manganese precursor, $KMnO_4$, simplifying the post-synthesis treatment and thereby increasing the viability in commercial applications. An environmental remediation application of C–NMOC was investigated using Pb(II) as the model pollutant. A nanostructured manganese oxide was also synthesized and its performance was compared with C–NMOC in removing Pb(II). The following conclusions were derived from the data.

- C–NMOC and NMO prepared through soft chemistry route are found to be excellent candidates for removing Pb(II) from aqueous solutions.
- As far as practical applicability is concerned, C–NMOC is more promising and is effective over a wide pH range compared to NMO. Reduced sensitivity to pH makes this adsorbent more attractive for cleaning up industrial effluents, especially effluents having low pH.
- The kinetics of Pb(II) removal by both C–NMOC and NMO are quick and the kinetic data can be well described by a pseudo-first-order equation. Sips model was found to be more suitable in describing the equilibrium data. Physisorption plays a significant role in the adsorption processes.
- A lower shift in the Mn 2p binding energy was found for supported manganese oxide in comparison to the unsupported material, indicating that support plays a role in deciding the exact oxidation state of Mn.
- Regeneration study reveals that the as-synthesized adsorbent can be used multiple times by treating the spent adsorbent by an acid like HCl.

## Acknowledgements

Authors thank EWRE Division, Department of Civil Engineering for providing analytical facilities for lead analysis. Other instrumentation was supported by the Unit on Nanoscience and Nanotechnology, IIT Madras, an initiative of the Department of Science and Technology (DST), India. We thank Lenzing AG, India for the generous gift of cellulose samples.

## Appendix A. Supplementary data

Supplementary data associated with this article can be found, in the online version, at doi:10.1016/j.jhazmat.2010.05.112.

## References

[1] E.C. Banks, L.E. Ferretti, D.W. Shucard, Effects of low level lead exposure on cognitive function in children: a review of behavioral, neuropsychological and biological evidence, Neurotoxicology 18 (1997) 237–281.

[2] J. Moros, I. Llorca, M.L. Cervera, A. Pastor, S. Garrigues, M. de la Guardia, Chemometric determination of arsenic and lead in untreated powdered red paprika by diffuse reflectance near-infrared spectroscopy, Anal. Chim. Acta 613 (2) (2008) 196–206.
[3] S. Tunali, T. Akar, A.S. Ozcan, I. Kiran, A. Ozcan, Equilibrium and kinetics of biosorption of lead(II) from aqueous solutions by *Cephalosporium aphidicola*, Sep. Purif. Technol. 47 (3) (2006) 105–112.
[4] K. Conrad, H.C.B. Hansen, Sorption of zinc and lead on coir, Bioresour. Technol. 98 (1) (2007) 89–97.
[5] E. Eren, B. Afsin, Y. Onal, Removal of lead ions by acid activated and manganese oxide-coated bentonite, J. Hazard. Mater. 161 (2–3) (2009) 677–685.
[6] A.S. Özcan, Ö. Gök, A. Özcan, Adsorption of lead(II) ions onto 8-hydroxy quinoline-immobilized bentonite, J. Hazard. Mater. 161 (1) (2009) 499–509.
[7] J.P. Ruparelia, S.P. Duttagupta, A.K. Chatterjee, S. Mukherji, Potential of carbon nanomaterials for removal of heavy metals from water, Desalination 232 (1–3) (2008) 145–156.
[8] L. Espinal, S.L. Suib, J.F. Rusling, Electrochemical catalysis of styrene epoxidation with films of $MnO_2$ nanoparticles and $H_2O_2$, J. Am. Chem. Soc. 126 (2004) 7676–7682.
[9] I.V. Mishakov, A.F. Betilo, R.M. Richards, V.V. Chesnokov, V. Vladimir, I. Zaikovskii, R.A. Buyanov, K.J. Klabunde, Nanocrystalline MgO as a dehydrohalogenation catalyst, J. Catal. 206 (1) (2002) 40–48.
[10] T. Pradeep, Anshup, Noble metal nanoparticles for water purification: a critical review, Thin Solid Films 517 (2009) 6441–6478.
[11] S.M. Maliyekkal, Anshup, K.R. Antony, T. Pradeep, High yield combustion synthesis of nanomagnesia and its application for fluoride removal, Sci. Tot. Environ. 408 (2010) 2273–2282.
[12] B.L. Cushing, V.L. Kolesnichenko, C.J. O'Connor, Recent advances in the liquid-phase syntheses of inorganic nanoparticles, Chem. Rev. 104 (9) (2004) 3893–3946.
[13] H. Chen, J. He, C. Zhang, H. He, Self-assembly of novel mesoporous manganese oxide nanostructures and their application in oxidative decomposition of formaldehyde, J. Phys. Chem. C 111 (49) (2007) 18033–18038.
[14] H. Chen, J. He, Facile synthesis of monodisperse manganese oxide nanostructures and their application in water treatment, J. Phys. Chem. C 112 (45) (2008) 17540–17545.
[15] V. Subramanian, H. Zhu, B. Wei, Alcohol-assisted room temperature synthesis of different nanostructured manganese oxides and their pseudo capacitance properties in neutral electrolyte, Chem. Phys. Lett. 453 (2008) 242–249.
[16] U. Vainio, K. Pirkkalainen, K. Kisko, G. Goerigk, E. Kotelnikova, R. Serimaa, Copper and copper oxide nanoparticles in a cellulose support studied using anomalous small-angle X-ray scattering, Eur. Phys. J. D 42 (2007) 93–101.
[17] H. Dong, J.P. Hinestroza, Metal nanoparticles on natural cellulose fibers: electrostatic assembly and in situ synthesis, ACS Appl. Mater. Interfaces 1 (4) (2009) 797–803.
[18] H. Junhui, K. Toyoki, N. Aiko, Facile *in situ* synthesis of noble metal nanoparticles in porous cellulose fibers, Chem. Mater. 15 (23) (2003) 4401–4406.
[19] R.V.S. Alfaya, Y. Gushikem, Aluminum oxide coated cellulose fibers modified with n-propylpyridinium chloride silsesquioxane polymer: preparation, characterization, and adsorption of some metal halides from ethanol solution, J. Colloid Interface Sci. 213 (2) (1999) 438–444.
[20] H.J. Fischer, K.H. Lieser, Syntheses of cellulose exchangers carrying chelating anchor groups for selective separation of uranyl ions, Angew. Makromol. Chem. 208 (1) (1993) 133–150.
[21] National Environment Protection Council (NEPC), Guideline on Laboratory Analysis of Potentially Contaminated Soils, Schedule B(3), 1999, available at: http://www.ephc.gov.au/pdf/cs/cs_03_lab_analysis.pdf.
[22] J.F. Moulder, W.F. Stickle, P.E. Sobol, K.D. Bomben, in: J. Chastain, R.C. King Jr. (Eds.), Handbook of X-ray Photoelectron Spectroscopy, Physical Electronics USA, Inc., 18725 Lake Drive East, Chanhassen, Minnesota 55317, USA, 1995.
[23] V.C.T. Costodes, H. Fauduet, C. Porte, A. Delacroix, Removal of Cd(II) and Pb(II) ions from aqueous solutions, by adsorption onto sawdust of *Pinus sylvestris*, J. Hazard. Mater. 105 (1–3) (2003) 121–142.
[24] R. Han, W. Zou, Z. Zhang, J. Shi, J. Yang, Removal of copper(II) and lead(II) from aqueous solution by manganese oxide coated sand. I. Characterization and kinetic study, J. Hazard. Mater. 137 (1) (2006)384–395.
[25] F. Kapteijin, A.D. van Langeveld, J.A. Moulijn, A. Andreini, M.A. Vuurman, A.M. Turek, J.M. Jehng, I.E. Wachs, Alumina-supported manganese oxide catalyst. Characterization: effect of precursor and loading, J. Catal. 150 (1994) 94–104.
[26] R. Radhakrishnan, S.T. Oyama, Electron transfer effects in ozone decomposition on supported manganese oxide, J. Phys. Chem. B 105 (2001) 4245–4253.
[27] C.H. Kuo, C.K. Lee, Enhancement of enzymatic saccharification of cellulose by cellulose dissolution pretreatments, Carbohydr. Polym. 77 (2009) 41–46.
[28] S. Liang, F. Teng, G. Bulgan, R. Zong, Y. Zhu, Effect of phase structure of MnO nanorod catalyst on the activity for CO oxidation, J. Phys. Chem. C 112 (2008) 5307–5315.
[29] W. Yantasee, C.L. Warner, T. Sangvanich, R.S. Addleman, T.G. Carter, R.J. Wiacek, G.E. Fryxell, C. Timchalk, M.G. Warner, Removal of heavy metals from aqueous systems with thiol functionalized superparamagnetic nanoparticles, Environ. Sci. Technol. 41 (14) (2007) 5114–5119.
[30] Y. Al-Degsa, M.A.M. Khraisheh, M.F. Tutunjib, Sorption of lead ions on diatomite and manganese oxides modified diatomite, Water Res. 35 (15) (2001) 3724–3728.
[31] L. Pauling, General Chemistry, Dover Publishing, 1970, p. 456.
[32] A.A. El-Bayaa, N.A. Badawy, E.A. Alkhalik, Effect of ionic strength on the adsorption of copper and chromium ions by vermiculite pure clay mineral, J. Hazard. Mater. 170 (2–3) (2009) 1204–1209.
[33] P.G. Tratnyek, R.L. Johnson, Nanotechnologies for environmental cleanup, Nano Today 1 (2) (2006) 44–48.
[34] S. S. Lagergren, Zur theorie der sogenannten adsorption gelöster stoffe, K Sven Ventenskapsakad Handl 24 (1898) 1–39.
[35] Y.S. Ho, G. McKay, Kinetic models for the sorption of dye from aqueous solution by wood, Process Saf. Environ. Protect. 76 (B2) (1998) 183–191.
[36] Y.S. Ho, G. McKay, The kinetics of sorption of divalent metal ions onto sphagnum moss peat, Water Res. 34 (3) (2000) 735–742.
[37] Y.S. Ho, Second-order kinetic model for the sorption of cadmium onto tree fern: a comparison of linear and non-linear methods, Water Res. 40 (1) (2006) 119–125.
[38] S.J. Allen, G. Mckay, J.F. Porter, Adsorption isotherm models for basic dye adsorption by peat in single and binary component systems, J. Colloid Interface Sci. 280 (2) (2004) 322–333.
[39] K. Vijayaraghavan, T.V.N. Padmesh, K. Palanivelu, M. Velan, Biosorption of nickel(II) ions onto *Sargassum wightii*: application of two-parameter and three-parameter isotherm models, J. Hazard. Mater. 133 (1–3) (2006) 304–308.
[40] W. Zou, R. Han, Z. Chen, J. Shi, L. Hongmin, Characterization and properties of manganese oxide coated zeolite as adsorbent for removal of copper(II) and lead(II) ions from solution, J. Chem. Eng. Data 51 (2) (2006) 534–541.
[41] A. Sari, M. Tuzen, D. Citak, M. Soylak, Adsorption characteristics of Cu(II) and Pb(II) onto expanded perlite from aqueous solution, J. Hazard. Mater. 148 (2007) 387–394.
[42] S.G. Wang, W.X. Gong, X.W. Liu, Y.W. Yao, B.Y. Gao, Q.Y. Yue, Removal of lead(II) from aqueous solution by adsorption onto manganese oxide-coated carbon nanotubes, Sep. Purif. Technol. 58 (1) (2007) 17–23.
[43] N. Boujelben, J. Bouzid, Z. Elouear, Studies of lead retention from aqueous solutions using iron-oxide-coated sorbents, Environ. Technol. 30 (7) (2009) 737–746.
[44] A. Sari, M. Tuzen, Removal of mercury(II) from aqueous solution using moss (*Drepanocladus revolvens*) biomass: equilibrium, thermodynamic and kinetic studies, J. Hazard. Mater. 171 (1–3) (2009) 500–507.
[45] J. Febrianto, A.N. Kosasih, J. Sunarso, Y.H. Ju, N. Indraswati, S. Ismadji, Equilibrium and kinetic studies in adsorption of heavy metals using biosorbent: a summary of recent studies, J. Hazard. Mater. 162 (2009) 616–645.